UNIVERSITY OF LEEDS

Article:
Nwobu, CJ orcid.org/0000-0003-0502-9841, Nakiganda, AM and Zhang, L (2017) Grid Voltage Synchronization for Unbalanced Voltages Using the Energy Operator. IEEE Journal of Emerging and Selected Topics in Power Electronics, 5 (3). pp. 1415-1424. ISSN 2168-6777

https://doi.org/10.1109/JESTPE.2017.2704022

Grid Voltage Synchronization for Unbalanced Voltages Using the Energy Operator

C. J. Nwobu, A.M. Nakiganda, and L. Zhang

Abstract--This paper presents a novel synchronization technique which can identify the grid voltage frequency and phase angle under unbalanced grid voltage conditions. The method combines the features of two different energy operator schemes: the basic one for estimating the frequency of the grid voltages and the cross-energy operator for phase tracking. Using a moving data window of five samples the algorithm can track the fundamental frequency and phase angle quickly and accurately. The paper discusses the fundamental principles of the method, highlights its features and filter requirements in implementation. An experimental implementation of this method is presented which validates its performance for practical operation. The ability of the proposed method to enable a STATCOM riding-through unbalanced grid voltage condition is verified by the results from a power network simulation study.

Index Terms—Frequency Estimation, Energy Measurement, Phase Lock Loop, Phase Measurements, Static VAR compensators

I. Introduction

Grid synchronization, involving detection of three-phase utility voltage frequency and phase angle, is of great importance to the power converters connected to the grid for the control of distributed generation, energy storage systems, power line conditioners and renewable energy sourced generators. In these applications, grid voltage imbalance may occur caused by asymmetrical transient faults [1-3] and this makes it challenging to synchronise the converters to the grid. It is however expected that under such conditions, a chosen synchronization scheme that is able to accurately identify and quickly lock on to the frequency and phase angle changes is used [4-7].

Grid synchronization techniques can be broadly categorized as closed-loop and open-loop types and for the former the most widely accepted scheme is the synchronous reference frame phase locked loop (SRF-PLL). This assumes perfectly balanced three-phase voltage, with equal amplitude, frequency and relative phase. Hence its equivalent rotating vector can be transformed into synchronously rotating reference form V_d and V_q. By feedback control of either of these two components, named also as loop filter, the phase angle can be identified. This method can be fast and accurate but cannot work for non-ideal conditions. For unbalanced voltage conditions [8], various schemes mostly modified from SRF-PLL method have been proposed. One of these applies additional filtering to remove the harmonic components from the d-q vectors [9-13]. Another approach extracts the fundamental positive sequence component (PSCs) initially using the Fortescue theorem [14-16]; it performs particularly well under unbalanced conditions, and hence has been the preferred method as it incurs the least time delays. Well-known schemes that use this method are the double synchronous reference frame (DDSRF-PLL) and cascaded delay signal cancellation (CDSC-PLL) [15, 16].

Open-loop methods, on the other hand, directly estimate the amplitude and phase of the grid voltage/current fundamental component through filtering the instantaneous samples of the measured voltage. Various methods identified in the literature include the space vector filter (SVF) [17]; Kalman filtering methods [18-21] and Least Square Estimation methods (WLSE) which has a fast response time and works well with frequency variations [20, 22-25]. The one regarded as the most stable open-loop method is based on the Discrete Fourier Transform (DFT) [24, 26], due to its extended data window length. The accuracy of all these methods can be affected by frequency variations and they are computationally intensive. Other approaches using interpolation (IpDFT) and recursive adaptive windows (RDFT) have been suggested and improve the computational efficiency [24, 26].

This paper proposes a different open-loop based technique, the energy operator synchronisation (EO-S), which can track the grid voltage fundamental frequency and phase angle variations under unbalanced conditions from only a few on-line samples of measured grid voltages. The rationale of the method, analogous to estimating the energy in a mechanical oscillator, is that the energy of a sinusoidal signal expressed by the product of amplitude and frequency squared can be estimated via a few consecutive samples. It provides a very fast estimate when the ratio of signal to additive noise is high, and does not require an extended data window length. Originated by Herbert M. Teager [27] and expounded by Kaiser [28], this technique has been applied widely and successfully in signal processing for the demodulation of speech signals [29]. In power applications, interest in it has

C. J. Nwobu is with the Electrical Engineering Department, University of Leeds, Leeds, LS29JT United kingdom, (e-mail: el08cjn@leeds.ac.uk).

A.M. Nakiganda is with the Electrical Engineering Department, University of Leeds, Leeds, LS29JT United kingdom, (e-mail: el14amn@leeds.ac.uk).

L. Zhang is with the Electrical Engineering Department, University of Leeds, Leeds, LS29JT United kingdom, (e-mail: l.zhang@leeds.ac.uk).

grown over the years. Most literature available investigates the energy operator for voltage flicker and amplitude change detection [26],[30-33]. More recent papers have proposed to use the technique for fault diagnosis of induction motors through demodulating the stator current before applying FFT analysis [34]. It has also been applied for online symmetrical component decoupling from three-phase voltages in combination with the Fortescue theorem[35]. The method has been tried recently for identification of real and reactive power changes, e.g. for measuring the power factor [36]. Application to estimating single phase grid frequency has also been reported [26, 37]. Hitherto, to the authors' knowledge, no literature has explored the application of the energy operator technique for power grid synchronization under unbalanced voltage conditions.

The proposed method combines two related energy operator schemes: the basic one for estimating the frequency of the grid phase voltages [28], and the cross-energy operator for relative phase angle identification [38-40]. Like the other open loop methods, the technique is sensitive to noise. However, this paper will show that with suitably chosen sampling frequency and carefully designed filters, the proposed EO algorithm is fast and accurate in tracking the grid voltage, and performs well. To validate its performance advantages an experimental test of the technique has been performed and will be presented in the paper. The time responses of the method under transient disturbances will be compared with two well-known PLL methods that also deal with unbalanced voltage due to grid faults. Moreover, the ability of the method to enable STATCOM devices to ride-through unbalanced voltages will be demonstrated via a simulation study of a power network using a STATCOM for combined reactive power and harmonic compensation.

II. Review Of Energy Operator

The Teager energy operator (TEO)[41] concept, introduced by H. M. Teager and J. F. Kaiser to calculate the energy needed to generate speech signals, can be applied as a basis for the determination of frequencies, phases and amplitudes of sinusoidal signals[36]. TEO synchronization in power systems is a time-domain technique that uses consecutive samples to efficiently track the instantaneous frequency and phase of waveforms such as line voltages and currents, without the need for adjusting controller parameters.

Teager's algorithm is used to estimate the energy in a time varying signal using adjacent samples[28]. The principle is derived from Newton's laws of motion applied to a conceptual un-damped mechanical oscillator described by $m\ddot{x}(t)+kx=0$, where the displacement is $x(t)=A\cos(\omega t+\phi_x)$ and the stored energy of the oscillator can be expressed as

$$E[x(t)]=\frac{1}{2}m\omega^2A^2 \tag{1}$$

where m = inertial mass, A and ω are the amplitude and angular frequency of the sinusoid. Energy is interchanged between kinetic and potential forms but its total is time-independent, and for any steady oscillation is proportional to the squared product of amplitude and frequency.

Applying this concept to the grid sinusoidal voltage of a power system with constant frequency and amplitude given as

$$v_x(t)=V_x\cos(\omega t+\phi_x) \tag{2}$$

the energy can be represented as

$$\begin{aligned}E[v_x(t)] &= \dot{v}_x^{\,2}(t)-v_x(t)\ddot{v}_x(t)\\ &= \left(-\omega V_x\sin(\omega t+\phi_x)\right)^2-\left(V_x\cos(\omega t+\phi_x)\right)\\ &\quad\times\left(-\omega^2V_x\cos(\omega t+\phi_x)\right)\\ &= \omega^2V_x^{\,2}\end{aligned} \tag{3}$$

The significance of expression (3) is that the amplitude-frequency product of a sinusoid can be found from time-localized estimates of the voltage and its first two time derivatives, with the result being independent of the instant at which the estimates are made. Extensions of the operator allow amplitude and frequency to be separated, and estimation of relative phase.

It is interesting that the term in (3) corresponding to potential energy is expressed in the form $-v_x(t)\ddot{v}_x(t)$ rather than as $\omega^2 v_x^{\,2}(t)$. Although these forms are numerically equal for a sinusoid, only the first of them can be estimated directly from the measured waveform without prior knowledge of ω.

In practice the instantaneous energy of a time varying voltage signal v_x must be estimated by using a discretized version of (3). This is derived from three equally spaced samples of the signal, assuming the general sample is given by

$$v_x(n)=V_x\cos(\Omega_x n+\phi_x) \tag{4}$$

where $\Omega_x=\frac{2\pi f}{f_s}$ is the discrete angle per sample, f is the signal frequency, f_s is the sampling frequency; hence the sample period $T_s=1/f_s$ and $\Omega_x = T_S\,\omega$. For high enough sampling frequency the discretized energy operator algorithm can be expressed as

$$\begin{aligned}E[v_x(n)] &= v_x(n)^2-v_x(n+1)v_x(n-1)\\ &= V_x^{\,2}\sin^2(\Omega_x)=V_x^{\,2}\,\Omega_x^{\,2}\\ &= V_x^{\,2}\,T_S^2\omega^2\end{aligned} \tag{5}$$

Equation (5) shows that with just three sample shifts of the original voltage signal, its instantaneous energy can be resolved. Thus for a high sampling frequency the instantaneous energy can be estimated in a time interval of $3T_S$.

III. Frequency Estimation

Expression (3) only yields an estimate of the amplitude – frequency product. The terms can be separated by applying the same operator to the derivative of the sinusoidal phase voltage $v_x(t)$. This will clearly yield an energy estimate of $\omega^4 v_x^{\,2}$, and then by eliminating v_x an estimator for the instantaneous angular frequency of $v_x(t)$ can be derived [29] . In discrete time, the discrete energy separation algorithm (DESA-2) [29] based on the weighted average of energies of each sample will

be employed. In this method the derivative of $v_x(n)$ defined by (4) can be approximated as the average of two finite differences i.e.

$$\dot{v}_x(n) \approx \frac{1}{2}\left(\frac{v_x(n+1)-v_x(n)}{T_s}+\frac{v_x(n)-v_x(n-1)}{T_s}\right) = \frac{v_x(n+1)-v_x(n-1)}{2T_s} \quad (6)$$

Substituting (4) into (6) gives

$$\dot{v}_x(n) \approx \frac{V_x\cos(\Omega_x(n+1)+\phi_x)-V_x\cos(\Omega_x(n-1)+\phi_x)}{2T_s} \quad (7)$$

which can be simplified using trigonometric identities to

$$\dot{v}_x(n) \approx V_x \sin(\Omega_x)\sin(\Omega_x n+\phi_x) \quad (8)$$

Applying (5) for energy in discrete time signals the energy $E[\dot{v}_x(n)]$ can be shown to be

$$E[\dot{v}_x(n)] = \dot{v}_x(n)^2 - \dot{v}_x(n+1)\dot{v}_x(n-1)$$

This can also be written in form of a three-sample symmetrical derivate as

$$E[\dot{v}_x(n)] = \left(\frac{v_x(n+1)+v_x(n-1)}{2T_s}\right)^2 - \left(\frac{v_x(n+2)+v_x(n)}{2T_s}\right)\cdot\left(\frac{v_x(n)+v_x(n-2)}{2T_s}\right) \quad (9)$$

The equation (9) shows that to estimate the energy of the derivate, a total number of 5 samples is required. This differs from the energy estimation in Section II which required 3 samples.

With further application of trigonometric identities using equations (5) and (8), this expression for the energy of the three-sample symmetrical derivative can be simplified to be

$$E[\dot{v}_x(n)] = V_x{}^2\sin^2(\Omega_x)\left(\sin^2(\Omega_x n+\phi_x) - \left(\sin(\Omega_x(n+1)+\phi_x)\times\sin(\Omega_x(n-1)+\phi_x)\right)\right)$$

$$E[\dot{v}_x(n)] = V_x{}^2\sin^2(\Omega_x n)\left(\sin^2(\Omega_x n+\phi_x) - \left(1-\sin^2(\Omega_x)+\sin^2(\Omega_x n+\phi_x)-1\right)\right)$$

$$E[\dot{v}_x(n)] = V_x{}^2\sin^4(\Omega_x) \quad (10)$$

Similar to the continuous time form an expression for the discrete angular frequency Ω_x can be deduced by taking the ratio of the energy of the discrete time voltage signal in (5) $E[v_x(n)]$ and energy of the voltage difference signals by (10), this gives

$$\frac{E[\dot{v}_x(n)]}{E[v_x(n)]} = \frac{V_x{}^2\sin^4\Omega_x}{V_x{}^2\sin^2\Omega_x} = \sin^2\Omega_x = \frac{1-\cos 2\Omega_x}{2}$$

$$f_x = \frac{1}{2\pi T_s}\sin^{-1}\left(\sqrt{\frac{E[\dot{v}_x(n)]}{E[v_x(n)]}}\right) \quad \text{or} \quad \frac{1}{4\pi T_s}\cos^{-1}\left(\sqrt{1-\frac{2E[\dot{v}_x(n)]}{E[v_x(n)]}}\right) \quad (11)$$

The frequency of the grid voltage can thus be determined with only five consecutive samples of the signal. A higher sampling frequency will thus enable better tracking of the frequency value, however, memory and computational requirements for the hardware involved should be put into consideration. Also, detection of frequency is dependent not on the peak magnitude of voltage but on the samples within the data window. This method estimates the frequency by using one single phase voltage signal. The sensitivity to noise introduced by the differential operator can be improved by using two phase voltage signals with an alternate form of the energy operator [42].

IV. Phase Estimation

Grid synchronization requires accurate and rapid estimation of phase difference as well as frequency. The TEO algorithm can also be used to determine the relative phase between two signals v_x and v_y. This is achieved by using energy cross products[36] , which for signals in discrete time form are given as

$$E[v_{xy}(n)] = v_x(n)v_y(n) - v_x(n+1)v_y(n-1) \quad (12)$$

$$E[v_{yx}(n)] = v_y(n)v_x(n) - v_y(n+1)v_x(n-1) \quad (13)$$

Since v_x is defined by (4) and the second signal is taken as:

$$v_y(n) = V_y\cos(\Omega_y n+\phi_y), \quad (14)$$

Equation (12) can be expressed as

$$E[v_{xy}(n)] = V_xV_y\left(\cos(\Omega_x n+\phi_x)\cos(\Omega_x n+\phi_y) - \cos(\Omega_x(n+1)+\phi_x)\cos(\Omega_x(n-1)+\phi_y)\right) \quad (15)$$

Applying trigonometric identities, this can be reduced to

$$E[v_{xy}(n)] = \frac{V_xV_y}{2}\left(\cos(\phi_x-\phi_y)-\cos(2\Omega_x+\phi_x-\phi_y)\right) = \frac{V_xV_y}{2}\left(\cos\theta_{xy}-\cos(2\Omega_x+\theta_{xy})\right) \quad (16)$$

The alternate expression obtained by interchanging variables is

$$E[v_{yx}(n)] = \frac{V_xV_y}{2}\left(\cos\theta_{xy}-\cos(2\Omega_x-\theta_{xy})\right) \quad (17)$$

It may be expected that the symmetrical expression obtained by averaging (16) and (17) will give lower noise errors in practice as it uses all 6 samples of the original signals, and it also leads to a simpler expression. With further trigonometric manipulation, the sum of both voltage discrete energies (16-17) can be simplified as

$$E[v_{xy}(n)]+E[v_{xy}(n)]=V_xV_y\cos\theta_{xy}(1-\cos2\Omega_x)$$
$$=2V_xV_y\cos\theta_{xy}\sin^2\Omega_x \quad (18)$$

Using expression (18) combined with the product of discrete energies $E[v_x(n)]$ and $E[v_y(n)]$ respectively from (5), one form of an expression can be derived which represents the phase angle difference $\theta_{xy} = \theta_y - \theta_y$ between both voltages:

$$\cos\theta_{xy}=\frac{2V_xV_y\cos\theta_{xy}\sin^2\Omega_x}{2V_xV_y\sin^2\Omega_x}=\frac{E[v_{xy}(n)]+E[v_{yx}(n)]}{2\sqrt{E[v_x(n)]\times E[v_y(n)]}} \quad (19)$$
$$\theta_{xy}=\cos^{-1}\left(\frac{E[v_{xy}(n)]+E[v_{yx}(n)]}{2\sqrt{E[v_x(n)]\times E[v_y(n)]}}\right)$$

This expression shows how the phase angle between the voltages, which may be two phase voltages of a three-phase grid system, can be estimated. This simple formula requires only 3 samples at the sampling frequency f_s.

V. The Energy Operator Synchronization Algorithm

Applying the solutions expressed in equations (11) and (19) above the energy operator phase locked loop algorithm is derived, with the implementation procedure as shown in Fig. 1 below.

A. EO-S Implementation Procedure

(1) The samples of the measured three phase voltages $V_a(t)$, $V_b(t)$ and $V_c(t)$ are placed in a moving data window, of five samples per phase (the minimum number of samples needed) in a first-in and first-out (FIFO) order, and processed using a chosen digital filter.

(2) The filtered three-phase data are Clarke transformed into their equivalent α-β components $v_\alpha(n)$ and $v_\beta(n)$ in a stationary reference frame. The α-β stationary reference frame makes it possible to track the arbitrary grid location. The serves as a reference to track the phase angled deviation between V_α and V_β under unbalance conditions as shown in Fig. 2.

(3) Using one of the three-phase voltages, say $V_a(n)$, and setting it as the reference $V_y(n)$. Evaluating the energies of $V_y(n)$ and $v_\alpha(n)$, and their energy cross product, hence obtaining $E[v_\alpha(n)]$, $E[\dot{v}_y(n)]$, $E[v_y(n)]$, $E[v_{\alpha y}(n)]$, $E[v_{y\alpha}(n)]$ using equations (5), (12), (13).

(4) Applying the results above to equations (11), (19), hence evaluating the frequency f_α and the phase difference $\theta_{\alpha y}$ (in this case $\theta_{\alpha a}$).

(5) Similarly, steps (3) and (4) can be done for $V_b(n)$ (Phase B) and $V_c(n)$ (Phase C) and setting them in turn as the reference $V_y(n)$ to get $\theta_{\alpha b}$ and $\theta_{\alpha c}$.

(6) Finally, updating with the corresponding phase angles from step (4) and (5) gives the phases θ_a, θ_b and θ_c, then integrating with the estimated frequency f_α creates a synchronized signal for each phase.

B. Features of the EO-S Scheme

Fig. 2 shows a graphical illustration of how the phase angles are estimated on an αβ stationary reference frame. The V_α vector acts as a reference that tracks the position of the a-b-c phase angles. The key feature of the technique lies in its ability for unbalanced voltage detection via concurrent evaluations of three-phase voltages for frequency and their relative phase angles. Under unbalanced conditions, the angular difference of 90° between V_α and V_β no longer holds, neither V_α is in phase with V_a as shown. Consequently the phase angle differences between V_α and V_{abc} vectors, $\theta_{\alpha a}$, θ_{ab}, θ_{ac}, deviate from the values at balanced conditions as shown in Fig 2(b). The EO-S algorithm evaluates these phase differences promptly using procedure (3) and (4) above and re-adjusts the phases at the final stage to align to the V_{abc} vectors.

This approach is not dependent on the voltage amplitude and would not require positive sequence extraction. In addition, as an open loop-based algorithm the EO-S is computationally efficient and faster in responding to grid frequency variation than other closed-loop approaches. Furthermore, this individual phase-angle based approach enables tracking of each single phase. This is particularly beneficial to the three-phase distribution systems where faults may occur at different phases.

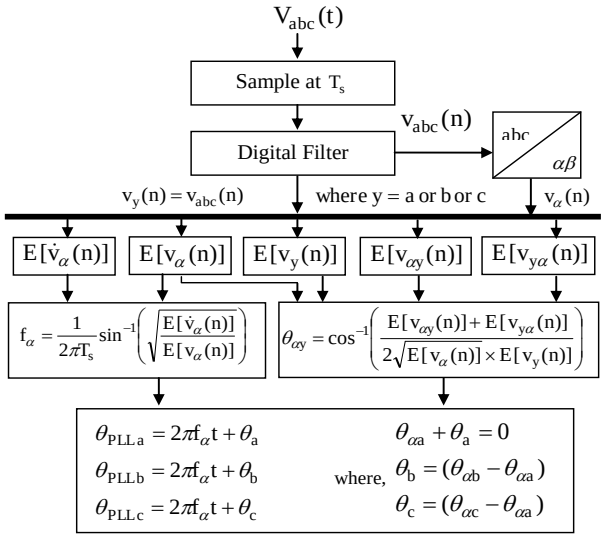

Fig. 1. Block diagram of the EO-S implementation

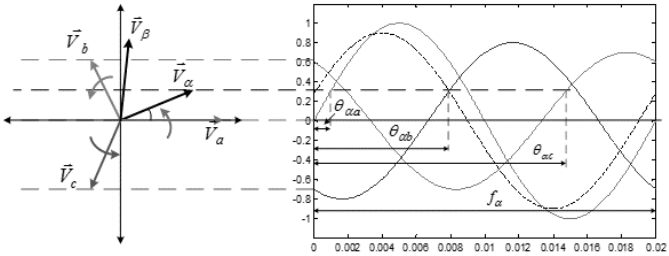

Fig. 2. Graphical illustration of the EO-S under Unbalanced Voltages

C. Filtering Requirement for EO-S

Being a sample-based technique, the EO-S is sensitive to

noise or harmonics, especially high frequency noise in the measured voltage signals [28]; thus it is necessary to process the samples using a suitable filter before performing the above described procedures. A compromise between fast response speed and high accuracy is the key design issue for digital filters, and often a trial and error approach is required.

For measured grid voltage samples a band pass filter centred at the nominal grid frequency is appropriate. Literature includes the use of moving average filters [36], and other digital filters including low order infinite-impulse-response (IIR) and finite-impulse-response (FIR) types. In this work, Recursive Discrete Fourier Transform (RDFT) and its inverse version (IRDFT) are used. This method assumes a nominal grid frequency f_g and extracts frequency components of the grid voltage samples. The DFT of the grid voltage at the (n-1)th and nth samples are used based on equations given by (20) and (21) respectively:

$$V_{f_g}(n-1) = \sum_{i=n-N}^{n-1} v(i)\, e^{-j\frac{2\pi i}{N} f_g} \tag{20}$$

$$V_{f_g}(n) = \sum_{i=n-N+1}^{n} v(i)\, e^{-j\frac{2\pi i}{N} f_g} \tag{21}$$

where v(i) are the voltage samples and N is the number of samples in one fundamental cycle. By subtracting (20) form (21) a recursive relationship can be obtained and the RDFT expressed as

$$V_{f_g}(n) = V_{f_g}(n-1) + \left(v(n) - v(n-N)\right) e^{-j\frac{2\pi i}{N} f_g} \tag{22}$$

The time-domain voltage value for the frequency equal f_g, which is the filtered grid voltage at the nth sample, can be obtained by taking inverse transformation, i.e. the IRDFT, of $V_{fg}(n)$ using

$$v_{f_g}(n) = \frac{1}{N} \sum_{n=0}^{N-1} V_{f_g}(n)\, e^{j\frac{2\pi n}{N}} \tag{23}$$

Cascading the RDFT of (22) and the IRDFT given by (23) implements a band pass filter for extracting f_g element in the grid voltage. Error may occur when N times the sample period is not equal to $1/f_g$ since the assumed f_g may not be exact. In this study f_g is set to 50 Hz. The computational burden of this filtering method is small compared with the standard DFT because it is recursive and only one frequency component is calculated. However, it will cause slower transient response when variations of input signal occur as they require at least one fundamental cycle window length to track the changes. This pre-filtering approach is good for achieving results with high accuracy under high harmonic distortion and can be used at higher sampling frequencies above 2 kHz. A simpler approach using a moving average filter (to be discussed in Section VII), would provide less precision but give acceptable results at lower sampling frequencies of 1 kHz or 2 kHz in cases of low harmonic distortion.

VI. Simulation Studies

A. Comparison with Two PLL schemes Under Unbalanced Voltage Grid Fault Conditions

The proposed EO-S scheme is now compared with DDSRF-PLL and CDSC-PLL in terms of response time, accuracy and computational efficiency. This comparison is based on ideal voltage conditions with no harmonic distortion.

Specimen voltage sags [43, 44] are based on recent IEEE guidelines. IEEE Std C37.242-2013 [43], with respect to previous clauses in IEEE std C37.118.1-2011 and IEC 61850-90-5 [43-45], details some requirements for phase monitoring units for unbalanced signals. A similar test approach is used here to compare response times of the three schemes.

Two network faults are investigated, the single phase grid fault (type B) resulting in a voltage sag of -20% at Phase A, and a phase to phase grid fault (type C) producing a voltage sag of -20% at both Phases B and C at a rated frequency of 50Hz.

The phasor diagrams for both cases are shown in Fig. 3. The proportional and integral gains of the P+I controllers in the DDSRF-PLL and CDSC-PLL are set to have the same bandwidth of 300Hz. All grid voltage measurements are normalized with respect to the base voltage. The sampling frequency for the EO-S is at 2 kHz. The RDFT is not used in this study.

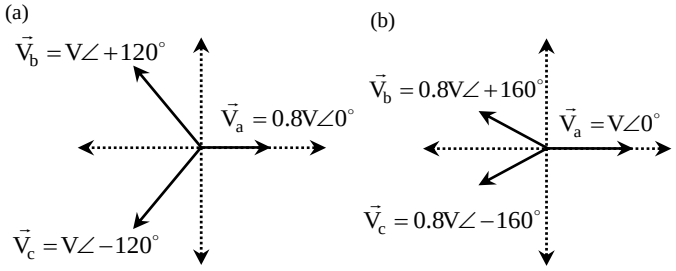

Fig. 3. (a) Single phase grid fault, (b) Phase to phase grid fault

a) Simulation Results - Type B Fault

Fig. 4 and Fig. 5 illustrate the results obtained for the three schemes to synchronize to the grid voltages under this fault condition. At time 0.2s, the grid fault occurs with a frequency variation of 0.1Hz. As expected there is a 20% voltage drop in Phase A to 0.8 pu. The DDSRF-PLL scheme is shown to settle down to steady state after 3 cycles (0.06s) whilst the CDSC-PLL settles within 2 cycles (0.04s). The CDSC-PLL is noisy mainly due the design stages of the delayed signal cancellation DSC_n operators (n =2, 8, 16). The resolution at each nth harmonic elimination stage takes place in the $\alpha\beta$ domain which affects the stability of the SRF-PLL. The EO-S is shown to be a better scheme since it shows the fastest response in tracking the frequency after 2.5 ms ($5\times T_s$) and phase change of the individual voltages after 1.5 ms ($3\times T_s$). The frequency spikes noticed in Fig 4 (d) and Fig. 5 are because of the processing of the erroneous samples noticed within the moving data window when the fault occurs. This depends on how severe the fault is and at what time instant it occurs. This depends also on the sampling frequency as a high frequency

may induce higher spikes. Hence, the EO-S is good for less dynamic frequency events such as such step changes over periods of times. The closed loop schemes would perform better in more dynamic frequency events such as in a nonlinear system.

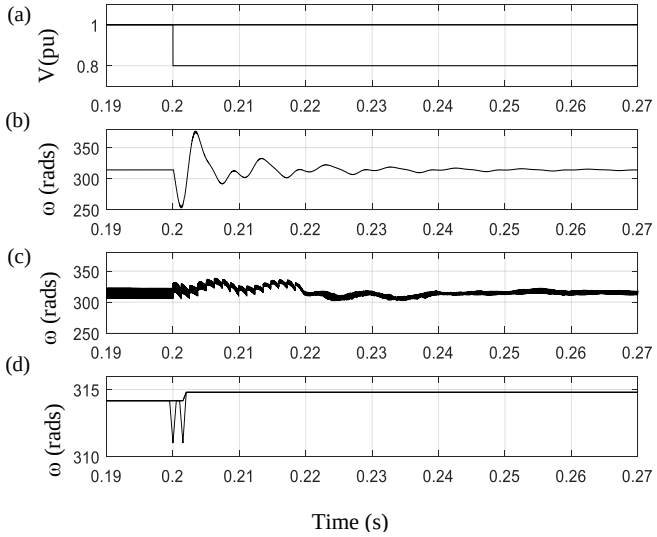

Fig. 4. Comparison of response times of schemes Sag B; (a) Peak Voltage (pu) (b) DDSRF-PLL, (c) CDSC-PLL, (d) EO-S

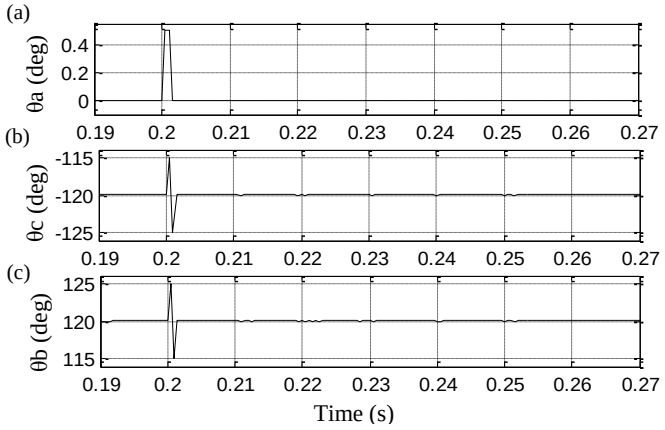

Fig. 5. EO-S Estimation of Phase Angle Sag (type B fault); (a) Phase A (deg) (b) Phase C (deg), (c) Phase B (deg)

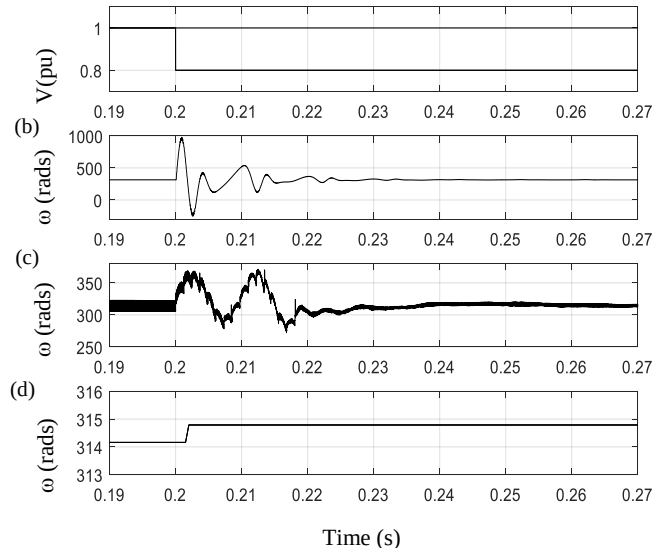

Fig. 6. Comparison of response times of schemes Sag C; (a) Peak Voltage (pu) (b) DDSRF-PLL, (c) CDSC-PLL, (d) EO-S

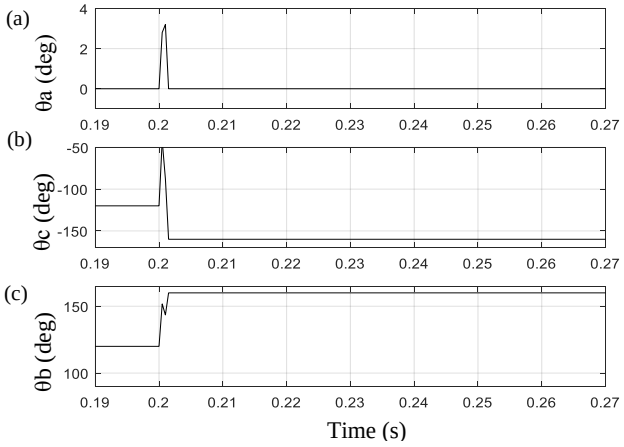

Fig. 7. EO-S Estimation of Phase Angle Sag C; (a) Phase A (deg) (b) Phase C (deg), (c) Phase B (deg)

b) Simulation Results - Type C Fault

Fig. 6 and Fig. 7 show the results the same three schemes under type C grid fault. The DDSRF-PLL scheme is seen to reach steady state after 3 cycles (0.06s) whilst the CDSC-PLL achieves this within 2 cycles (0.04s). Similarly, the EO-S is shown to be superior, since it has the fastest response speed in tracking the frequency after 2.5 ms ($5\times T_s$) and phase change of the individual voltages within 1.5 ms ($3\times T_s$).

B. Performance with Voltage Harmonic Distortion

A combined EO-S scheme with a RDFT filter discussed in Section V can provide a solution for synchronization for voltage corrupted with harmonic noise. These are now investigated in terms of response time and accuracy. The harmonic distortions injected on these voltages were based on IEC 61000-3-6 compatibility level standards for low and medium voltage networks [46]. The data sampling frequency is fixed at 5 kHz.

Fig.8 shows an example of unbalanced three-phase voltages and their corresponding waveforms after being processed by the RDFT filter. At time 0.06s, step changes in magnitudes of -20% and -50% are imposed on Phases B and C voltages respectively. As can be seen in Fig.8 (c) after a time delay of 0.021 s (one fundamental cycle + $5\times T_s$) the frequency estimation is completed and in Figs.8 (e)-(g) estimations of three phase angles are converged within a duration of 0.0206s (one fundamental cycle + $3\times T_s$). These results highlight the fact that the time required for implementing EO-S algorithm is significantly shorter than that of RDFT. The total response time for this algorithm is mainly due to the duration of the RDFT window.

a) Computational Complexity

Based on the implementation of the SIMULINK models used in the above investigations, the complexity of each scheme is summarized in Table I. In terms of simple arithmetic calculations EO-S has a higher number of operations than that of DDSRF, but is significantly less than CDSC. It uses least number of trigonometric calculations; consequently, the response time for the EO-S is also significantly faster compared to both DDSRF and CDSC

schemes. The DDSRF and CDSC are closed loop systems and the response time depends mainly on the bandwidth of the P+I controllers in the PLL. In the case of the EO-S, this is an open loop system and the response time is the width of moving data window ($5\times T_s$) plus the delay time added by the filter.

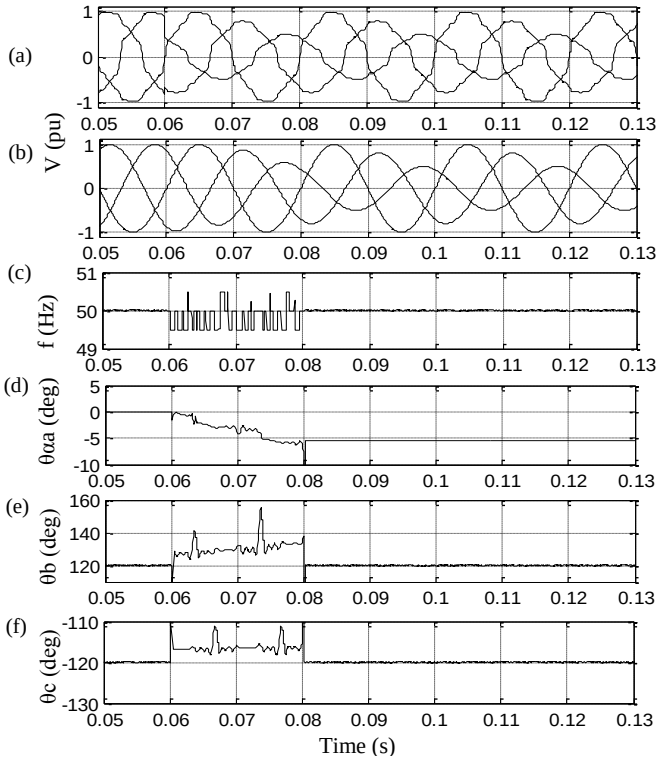

Fig. 8. (a) Voltage with harmonics, (b) Voltage after RDFT, (c) frequency detection, (d) –(f) Phase detection (A,B,C)

TABLE I
Comparisons of Computational Complexity & Response times

Method	Number of Operations		Response Time
	Arithmetic	Cos and Sine	
EO-S (f)	30	7	0.0225s
DDSRF	17	8	0.06s
$CDSC_{2,8,16}$	76	16	0.04s

C. Control of STATCOM under Unbalanced Grid Voltages

The effectiveness of the EO-S is tested by applying it to a STATCOM which uses a three-phase voltage-source converter and is shunt-connected to the load side bus – the point of common coupling (PCC) - as shown in Fig. 9. It should simultaneously supply the load reactive power and eliminate current harmonics. The power network consists of a line load of 80 kVA with power factor 0.8 and a thyristor controlled load of 40 kVA, while the firing angle is set to 30°; the parameters for the STATCOM device are fs = 5kHz, V_{DC} = 800V with a 1.8Ω, 5mH R-L filter at the AC side. The test verifies the STATCOM performance under two conditions: unbalanced voltages at the PCC in the network and reactive power compensation whilst in active filtering mode under balanced voltage conditions. Since these abnormalities may last for a short time, it is expected that, with the EO-S scheme, the STATCOM can maintain operation until the grid voltage unbalance is cleared.

The STATCOM uses conventional P+I integral control for DC bus capacitor balancing and a deadbeat predictive current control scheme with an additional control to extract reactive and harmonic current including negative sequence components due to unbalanced voltage from measured load current as depicted as a block diagram in Fig.10.

This is the most important part of the control scheme which relies on EO-S to identify the grid voltage phase angle θ and functions as a high pass filter as follows: With θ value the scheme converts the measured three-phase load currents to their equivalent d-q elements in synchronous reference frame, i_{ld} and i_{lq} . These are then applied to a low pass filter (LPF shown in Fig. 10 to cancel all AC current components leaving only the fundamental positive sequence elements, i_{fd} and i_{fq} . Subtracting these from the original i_{ld} and i_{lq} , the harmonic current components, i_{hd} and i_{hq} in the original measured currents are then extracted including negative sequence element as it appeared second harmonic. These extracted current components are subsequently transformed back to their equivalent three phase quantities and set as references for harmonic current control. For reactive current control, the fundamental reactive current component i_{fq} provides reference value. Thus the total reference current for harmonics and reactive current control in d-q form is obtained as:

$$\begin{bmatrix} i_d^* \\ i_q^* \end{bmatrix} = \begin{bmatrix} \tilde{i}_d \\ \bar{i}_q + \tilde{i}_q \end{bmatrix} = \begin{bmatrix} i_{hd} \\ i_{fq} + i_{hq} \end{bmatrix} \qquad (24)$$

Clearly the performance of the above scheme is dependent on the accurate tracking of the grid voltage vector by the EO-S and the optimal tuning of the LPF parameters. The LPF considered should ensure a balance between good attenuation characteristics to ensure better accuracy and fast time response with low overshoot. A second-order Butterworth filter was implemented.

The level of system abnormality is set by assuming that the three-phase voltage at the PCC is unbalanced at the level of 75% with positive sequence voltage $V^+ = 0.2\angle -25°$ and negative $V^- = 0.15\angle 35°$ introduced in the system at 0.3s. Such a disturbance could arise from a single phase fault in a remote network sharing a bus with the PCC. The performance of the STATCOM compensation characteristic under this case

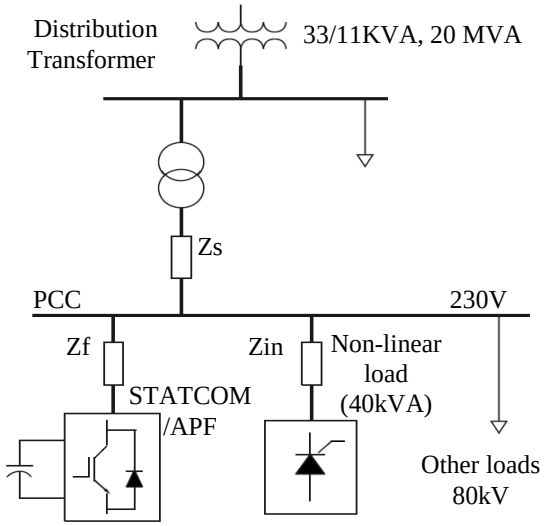

Fig. 9. Simulated Power system + STATCOM model

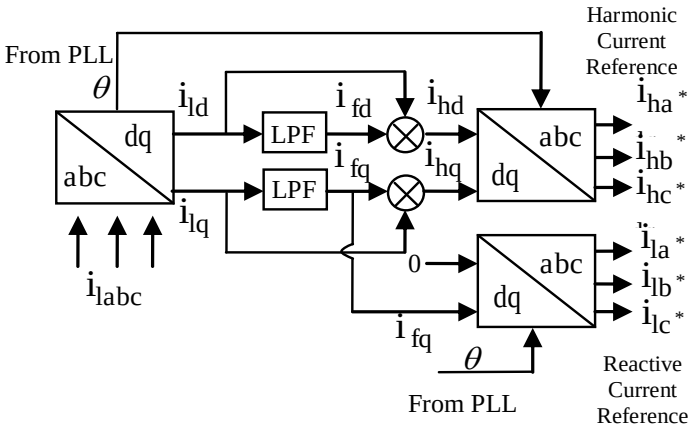

Fig. 10. STATCOM Current Control Scheme

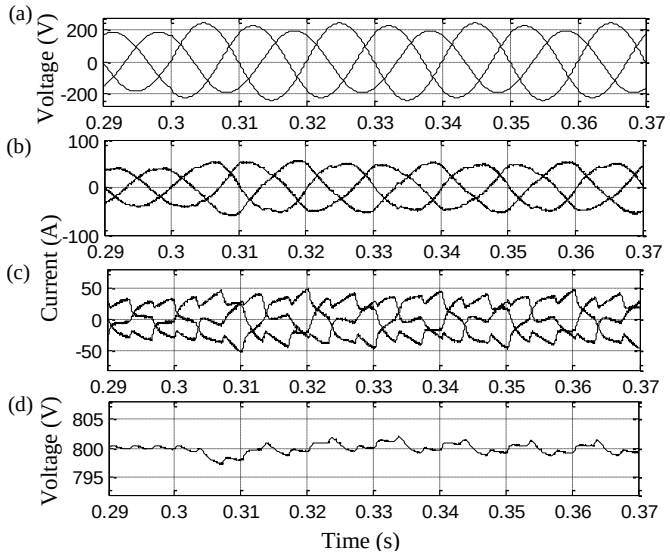

Fig. 11. Simulation with unbalanced supply voltage using EO-S: a) supply voltage, b) supply current, c) compensating filter current d) DC link voltage

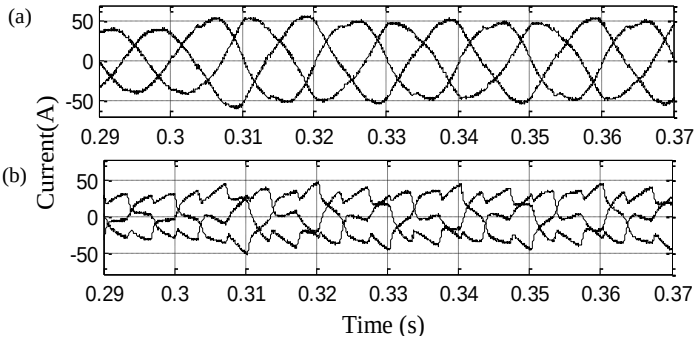

Fig. 12. Simulation with unbalanced supply voltage using SRF-PLL: a) supply current, b) compensating filter current,

with the EO-S (Fig.11) is compared with that when SRF-PLL (Fig.12) is employed.

Fig.11 shows unbalanced supply voltages culminating in the flow of unbalanced currents for a short time period. The STATCOM has been controlled to ride-through the fault whilst compensating for the harmonics Fig.11 (b). In this case active power filtering control ensures compensation of both the positive and negative sequence harmonics however does not provide for the compensation of the unbalanced PCC currents or voltage. This may be realised by decoupling the control of both negative and positive sequence control and subsequent elimination of the negative sequence components.

With the similar conditions applied to the system with STATCOM using the conventional SRF-PLL for synchronization, the supply currents, Fig.11 (b), are observed to be highly degraded with a THD level of 9.4% which exceeds recommended IEEE 519 standard [47] .

In both cases, however, a high DC ripple is observed. In[48], it was noted that the flow of unbalanced compensating currents due to the presence of negative sequence fundamental components, causes a second order harmonic to arise on the DC-link of the converter. This harmonic in turn leads to a 3rd-order harmonic in the supply currents if uncompensated.

Fig. 13 (a)-(e) show the performance under transient changes in firing angle from 30° to 60° of the thyristor bridge at 0.8s illustrating both harmonic mitigation and reactive power compensation. In this scenario synchronization is achieved promptly enabling unity power factor compensation

.

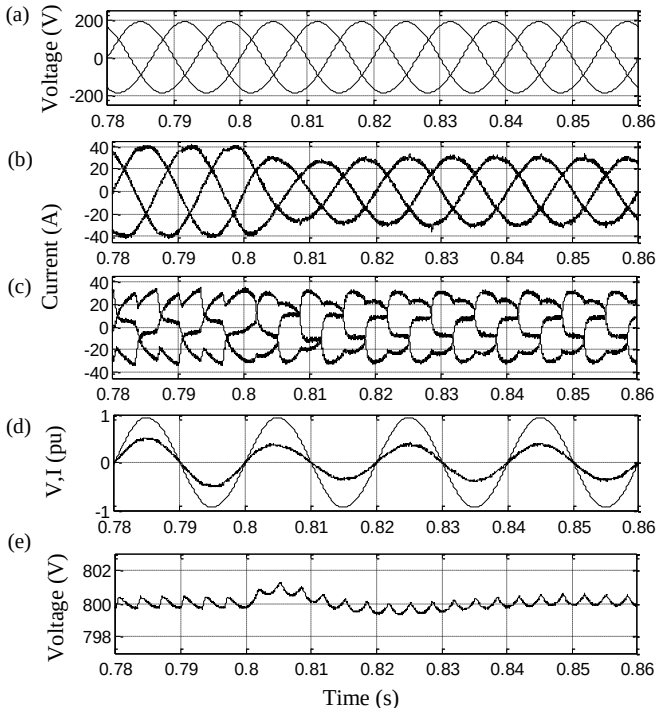

Fig. 13. Reactive power compensation with transient change in the thyristor firing angle from 30° to 60°: a) supply voltage, b) supply current, c) compensating filter current, d) supply power factor e) DC link voltage

VII. Experimental Study

The performance of the EO-S synchronization technique has been verified experimentally using a practical setup, as shown in Fig. 14. This consists of a 96 MHz mbed NXP LPC1768 microcontroller as an AC voltage generator for 50Hz 3-phase voltage signals, and a 120 MHz EA NXP LPC4088 microcontroller acting as the control unit and is able to provide high enough resolution and sample rate for the internal A2D converters. In this study, phase estimation is validated by the phase deviation caused between the α-β voltage vectors and frequency estimation using the v_α voltage vector.

The ability of the EO-S scheme is investigated under both balanced and unbalanced voltages. In this study, the data sampling frequency is fixed at 1 kHz and a moving average filter at 10 sample instants is used at the digital filtering stage to reduce the noise to achieve more accurate results. This introduces a delay response of at least 10 ms under transient changes.

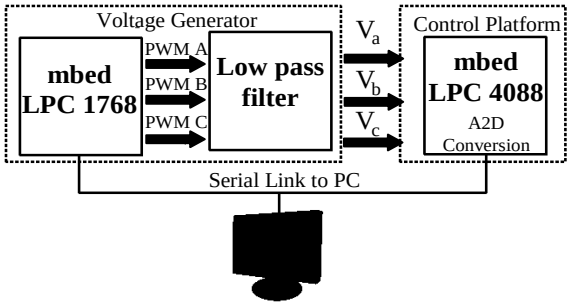

Fig. 14. EO-S hardware test circuit setup

A. Voltage Generator

The LPC1768 micro-controller was programmed to generate variable 3-phase voltages to introduce grid conditions of frequency and phase change, and voltage imbalance. This imitates the same response you will expect from the voltage output (±5V) of transducers measuring the voltages changes of a practical three-phase network. This is done by generating a 20 kHz PWM signal via the 5V analogue output pins. In other to see the actual voltage signal, a RC low pass filter is constructed at a cut off frequency of 60Hz with component values chosen as R= 8kΩ, C = 0.33μF. By changing the modulation index and frequency using interrupts and a sine look up table, this emulates the characteristics of the AC grid voltage required under fault conditions.

B. Filtering Requirements

The choice of the filter at the pre-filtering stage depends mainly on the low and high frequency harmonics present in the sinusoidal voltages and the A/D sampling frequency. Since the EO-S is a sample based technique, it is prone to noise and there is a trade-off between sampling frequency, filter choice and time delays. The higher sampling frequencies are more sensitive to changes and additional time delays are mainly dependent on the choice of digital filters. Lower sampling frequencies are less sensitive and accuracy can be improved with simple filters like moving average filter (MAF) but with additional time delays.

The RDFT as discussed earlier in Section V has been successfully implemented as filter and shown to handle high sampling frequency estimations with energy operator. This is mainly because it can be used as a selective band pass filter with a narrow frequency bandwidth. Although this works well at high frequencies, there is still an imminent one cycle delay (20ms). Alternatively, a simple moving average filter can achieve less precision but acceptable results at much lower sampling frequencies provided the voltage are not distorted.
In this experiment, a simple moving average filter is used and programmed within the mbed LPC 4088 control platform at a low sample frequency. This averages the calculated frequency and phase estimations over a number of sample steps. For best performance in this operation, a sampling frequency of 1 kHz or 2 kHz is recommended. This frequency is able to provide sufficient results for this analysis. The accuracy can be improved by extending the moving average filter to average more samples at the expense of increased time delays.

C. Performance with Balanced Three-Phase Voltages

Fig.15 shows the frequency and phase angle estimated by the EO-S algorithm. Fig 15 (a) show a 10 second representation of the estimated frequency at which at time 19.98s there is a step change from 50Hz – 55Hz. This is reflected in 4 cycle representation of the three phase voltages in Fig 15 (d). At the time intervals $19.94 < t < 19.98$, the voltages are balanced and the EO-S algorithm responds to track the frequency of 50Hz. At time instant t = 19.98s, the frequency of the three-phase voltages is raised from 50 to 55Hz, the EO-S algorithm responds and the frequency

converges quickly to the correct value as shown in Fig 15 (b). Though there is a ripple of ±1 Hz observed due to the noise remaining in the voltage signal even with the use of the moving average filter. The phase angle estimation gives the angle between Phase A (V_α) and V_β vectors derived from α-β transformation of the 3-phase voltage waveforms. As can be seen in Fig 15 (c), the angular difference is kept to be 1.57 rads (90°) since the three-phase voltages are well-balanced. The small phase ripple of approximately ± 0.03 rads can be noticed and is also due to the noise in the measured data. The settling time of approximately 10 ms is observed which is faster compared to the RDFT method used in Section V.

Fig. 16 shows the nature of the estimations without the moving average filter. The response times are faster within 5ms but compared to Fig.15 the waveforms are shown to have more noise. The frequency ripple observed is now within ± 5Hz and the phase ripple larger at ±0.1 rads.

D. Performance with Unbalanced Three-Phase Voltages

To investigate the EO-S's capability of tracking unbalanced grid voltage, the generated three-phase voltages were varied with a 50% and 80% magnitude reductions respectively in phase-B and phase-C voltages at 50.08 s as shown in Fig.17(f) and back to the balanced case at 60.08s as shown in Fig 17 (g). The technique is seen to accurately track the frequency and phase in each case. As the voltage is unbalanced and phase unsymmetrical, the measured phase value changes from the ideal 1.57 rads to 1.8 rads as shown in Fig 17 (c). The result converges quickly to the correct phase value within 10 ms (Fig. 17(d)-(e)). The phase and frequency ripple observed are the same as that of previous case with a frequency and phase ripple of ±1 Hz and ±0.03 rads respectively.

Fig. 18 shows the same results but with no moving average filter. Compared to Fig. 17 the waveforms are shown have more noise and the frequency ripple is at ± 5Hz and the phase ripple larger at ±0.1 rads. This is reflected in both the frequency and phase estimation.

VIII. Conclusion

A novel EO-S technique has been presented and its principle and implementation procedures were explained. This open-loop synchronization scheme combines two different EO operations and has been shown to achieve fast and accurate detection of frequency and phase angle when combined with an appropriate filter. Comparative studies of this technique with two other well-known closed-loop PLL schemes have been performed under two unbalanced voltage conditions. Results have shown that the EO-S outperformed the others in terms of fast response speed and accuracy in tracking. Further validation of this technique has been carried out by applying it to a STATCOM for current control under unbalanced voltage operations. The results obtained were shown to be better than the conventional SRF-PLL. Finally, a hardware implementation of this EO-S has also been reported in the paper, showing the simplicity of the method.

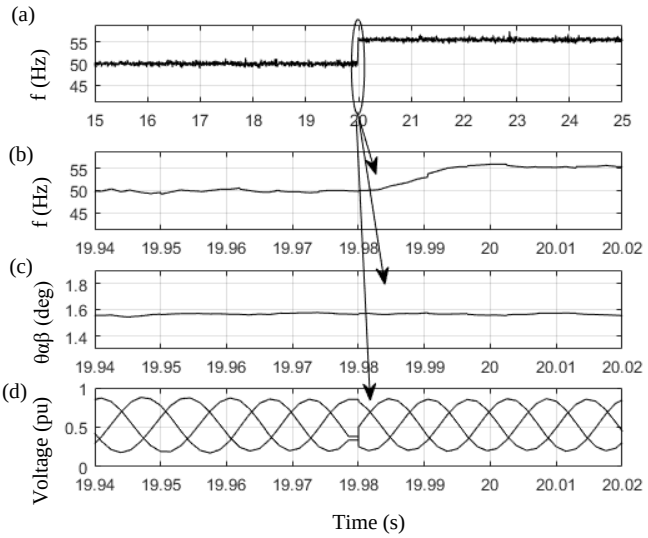

Fig. 15. Detected result for change in frequency from 50-55 Hz with a 10 sample moving average filter: (a)-(b) estimated frequency at step change, (c) estimated phase, d) Generated 3-phase voltage

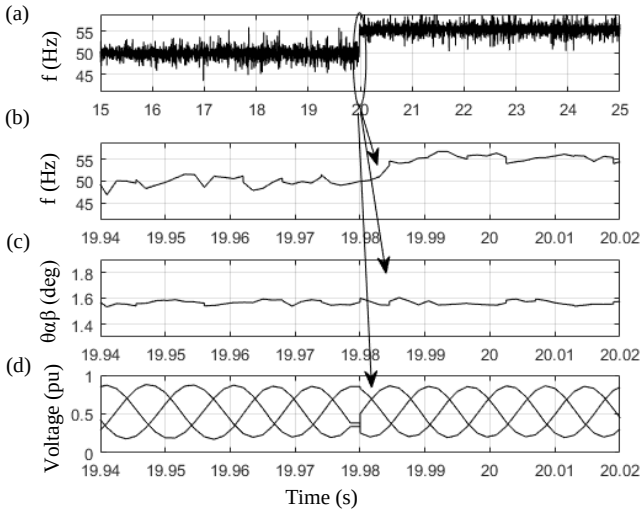

Fig. 16. Detected result for change in frequency from 50-55 Hz with no moving average filter: (a)-(b) estimated frequency at step change, (c) estimated phase, d) Generated 3-phase voltage

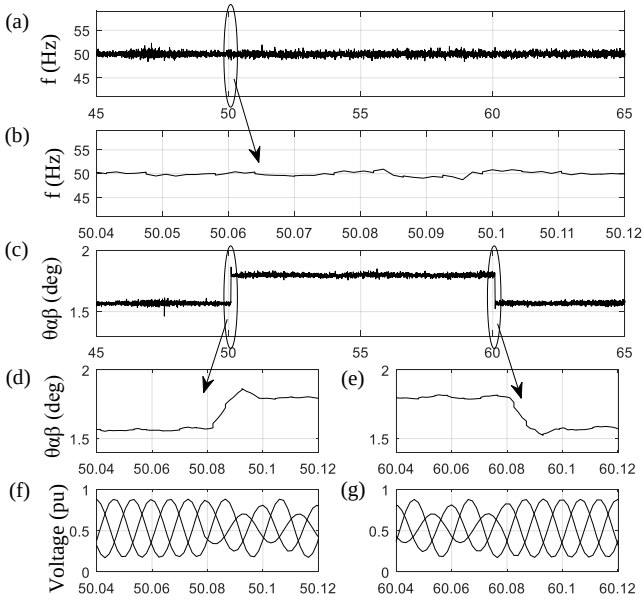

Fig. 17. Detected result for 50% and 80% reduction in phase-B and phase-C respectively with a 10 sample moving average filter: (a)-(b) estimated frequency, (d)-(e) estimated phase, (f)-(g) Generated 3-phase voltage at step change

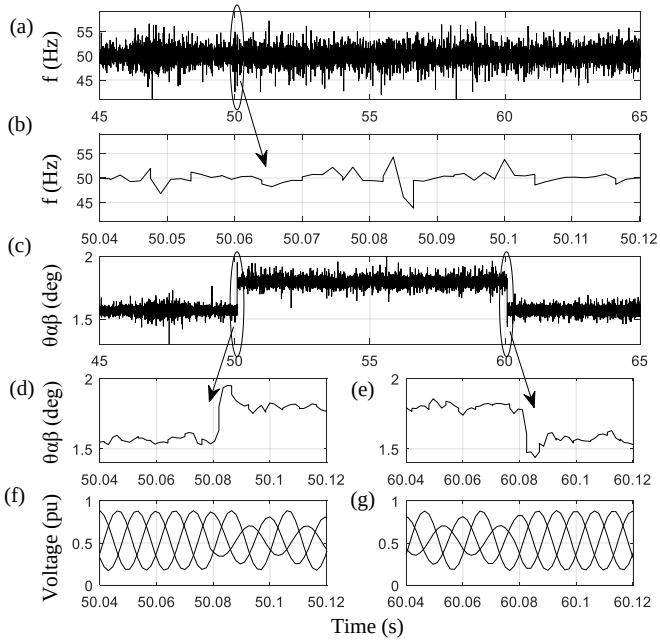

Fig. 18. Detected result for 50% and 80% reduction in phase-B and phase-C respectively (no moving average filter): (a)-(b) estimated frequency, d)-(e) estimated phase, (f)-(g) Generated 3-phase voltage at step change

IX. References

[1] M. F. McGranaghan, D. R. Mueller, and M. J. Samotyj, "Voltage sags in industrial systems," Industry Applications, IEEE Transactions on, vol. 29, pp. 397-403, 1993.

[2] J. Wang, S. Chen, and T. T. Lie, "System voltage sag performance estimation," Power Delivery, IEEE Transactions on, vol. 20, pp. 1738-1747, 2005.

[3] J. A. Martinez and J. Martin-Arnedo, "Voltage sag studies in distribution Networks-part I: system modeling," Power Delivery, IEEE Transactions on, vol. 21, pp. 1670-1678, 2006.

[4] Y. Yongheng, F. Blaabjerg, and Z. ZhiXiang, "Benchmarking of Grid Fault Modes in Single-Phase Grid-Connected Photovoltaic Systems," Industry Applications, IEEE Transactions on, vol. 49, pp. 2167-2176, 2013.

[5] J. V. Milanovic and Z. Yan, "Global Minimization of Financial Losses Due to Voltage Sags With FACTS Based Devices," Power Delivery, IEEE Transactions on, vol. 25, pp. 298-306, 2010.

[6] Z. Yan, Milanovic, x, and J. V., "Global Voltage Sag Mitigation With FACTS-Based Devices," Power Delivery, IEEE Transactions on, vol. 25, pp. 2842-2850, 2010.

[7] Milanovic, x, J. V., and Z. Yan, "Modeling of FACTS Devices for Voltage Sag Mitigation Studies in Large Power Systems," Power Delivery, IEEE Transactions on, vol. 25, pp. 3044-3052, 2010.

[8] "IEEE Standard Definitions for the Measurement of Electric Power Quantities Under Sinusoidal, Nonsinusoidal, Balanced, or Unbalanced Conditions," IEEE Std 1459-2010 (Revision of IEEE Std 1459-2000), pp. 1-50, 2010.

[9] L. Shi and M. L. Crow, "A novel PLL system based on adaptive resonant filter," in Power Symposium, 2008. NAPS'08. 40th North American, 2008, pp. 1-8.

[10] E. Robles, S. Ceballos, J. Pou, J. L. Martin, J. Zaragoza, and P. Ibanez, "Variable-frequency grid-sequence detector based on a quasi-ideal low-pass filter stage and a phase-locked loop," IEEE transactions on power electronics, vol. 25, pp. 2552-2563, 2010.

[11] E. Courbon, S. Poullain, and J. Thomas, "Analysis and synthesis of a digital high dynamics robust PLL for VSC-HVDC robust control," in 10th European Conference on Power Electronics and Applications, 2003.

[12] A. Nicastri and A. Nagliero, "Comparison and evaluation of the PLL techniques for the design of the grid-connected inverter systems," in 2010 IEEE International Symposium on Industrial Electronics, 2010, pp. 3865-3870.

[13] G. Saccomando and J. Svensson, "Transient operation of grid-connected voltage source converter under unbalanced voltage conditions," in Industry Applications Conference, 2001. Thirty-Sixth IAS Annual Meeting. Conference Record of the 2001 IEEE, 2001, pp. 2419-2424.

[14] B. V. P. Chong, K. W. Lee, and L. Zhang, "Voltage synchronisation techniques for grid-connected power converters," in Power Electronics, Machines and Drives (PEMD 2014), 7th IET International Conference on, 2014, pp. 1-6.

[15] P. Rodriguez, J. Pou, J. Bergas, J. I. Candela, R. P. Burgos, and D. Boroyevich, "Decoupled double synchronous reference frame PLL for power converters control," IEEE Transactions on Power Electronics, vol. 22, pp. 584-592, 2007.

[16] Y. F. Wang and Y. W. Li, "Grid Synchronization PLL Based on Cascaded Delayed Signal Cancellation," IEEE Transactions on Power Electronics, vol. 26, pp. 1987-1997, 2011.

[17] J. Svensson, "Synchronisation methods for grid-connected voltage source converters," IEE Proceedings-Generation, Transmission and Distribution, vol. 148, pp. 229-235, 2001.

[18] R. Cardoso, R. F. De Camargo, H. Pinheiro, and H. Grundling, "Kalman filter based synchronisation methods," IET generation, transmission & distribution, vol. 2, pp. 542-555, 2008.

[19] V. M. Moreno, M. Liserre, A. Pigazo, and A. Dell'Aquila, "A comparative analysis of real-time algorithms for power signal decomposition in multiple synchronous reference frames," IEEE Transactions on Power Electronics, vol. 22, pp. 1280-1289, 2007.

[20] M. Padua, S. Deckmann, G. Sperandio, F. Marafao, and D. Colon, "Comparative analysis of synchronization algorithms based on PLL, RDFT and Kalman filter," in 2007 IEEE International Symposium on Industrial Electronics, 2007, pp. 964-970.

[21] A. A. Girgis, W. B. Chang, and E. B. Makram, "A digital recursive measurement scheme for online tracking of power system harmonics," IEEE transactions on Power Delivery, vol. 6, pp. 1153-1160, 1991.

[22] H.-S. Song, H.-g. Park, and K. Nam, "An instantaneous phase angle detection algorithm under unbalanced line voltage condition," in Power Electronics Specialists Conference, 1999. PESC 99. 30th Annual IEEE, 1999, pp. 533-537.

[23] M. Karimi-Ghartemani and M. R. Iravani, "A method for synchronization of power electronic converters in polluted and variable-frequency environments," IEEE Transactions on Power Systems, vol. 19, pp. 1263-1270, 2004.

[24] F. Baradarani, M. R. Dadash Zadeh, and M. A. Zamani, "A Phase-Angle Estimation Method for Synchronization of Grid-Connected Power-Electronic Converters," Power Delivery, IEEE Transactions on, vol. 30, pp. 827-835, 2015.

[25] E. Demeter, "A digital relaying algorithm for integrated power system protection and control," University of Saskatchewan Saskatoon, 2005.

[26] M. S. Reza, M. Ciobotaru, and V. G. Agelidis, "Single-Phase Grid Voltage Frequency Estimation Using Teager Energy Operator Based Technique," Emerging and Selected Topics in Power Electronics, IEEE Journal of, vol. PP, pp. 1-1, 2015.

[27] H. M. Teager and S. M. Teager, A Phenomenological Model for Vowel Production in the Vocal Tract: College-Hill Press, 1983.

[28] J. F. Kaiser, "On a simple algorithm to calculate the `energy' of a signal," in Acoustics, Speech, and Signal Processing, 1990. ICASSP-90., 1990 International Conference on, 1990, pp. 381-384 vol.1.

[29] P. Maragos, J. F. Kaiser, and T. F. Quatieri, "Energy separation in signal modulations with application to speech analysis," Signal Processing, IEEE Transactions on, vol. 41, pp. 3024-3051, 1993.

[30] F. Li, Y. Gao, Y. Cao, and R. Iravani, "Improved Teager Energy Operator and Improved Chirp-Z Transform for Parameter Estimation of Voltage Flicker," Power Delivery, IEEE Transactions on, vol. PP, pp. 1-1, 2015.

[31] S. Hong and W. Yi, "Detection of Voltage Flicker Based on Mathematical Morphology Filter and Teager Energy Operator," in Power System Technology, 2006. PowerCon 2006. International Conference on, 2006, pp. 1-6.

[32] M. A. Eldery, E. F. El-Saadany, and M. M. A. Salama, "A simple energy operator computational method for voltage flicker assessment," Power Delivery, IEEE Transactions on, vol. 21, pp. 1743-1750, 2006.

[33] T. K. Abdel-Galil, E. F. El-Saadany, and M. M. A. Salama, "Online tracking of voltage flicker utilizing energy operator and Hilbert transform," Power Delivery, IEEE Transactions on, vol. 19, pp. 861-867, 2004.

[34] M. Pineda-Sanchez, R. Puche-Panadero, M. Riera-Guasp, J. Perez-Cruz, J. Roger-Folch, J. Pons-Llinares, et al., "Application of the Teager–Kaiser Energy Operator to the Fault Diagnosis of Induction Motors," Energy Conversion, IEEE Transactions on, vol. 28, pp. 1036-1044, 2013.

[35] M. A. Eldery, E. F. El-Saadany, and M. M. A. Salama, "An on-line measurement of symmetrical components utilizing the energy operator," in Power Engineering Society General Meeting, 2006. IEEE, 2006, p. 5 pp.

[36] D. A. Kaiser and J. F. Kaiser, "Estimation of power systems amplitudes, frequencies, and phase characteristics using Energy Operators," in Energy Conversion Congress and Exposition (ECCE), 2012 IEEE, 2012, pp. 930-937.

[37] C. J. Nwobu and L. Zhang, "Lifting wavelet transform and energy operator synchronization for a flying capacitor multi-level inverter based active power filter," in Power Electronics and Applications (EPE), 2013 15th European Conference on, 2013, pp. 1-10.

[38] A.-O. Boudraa, S. Benramdane, J.-C. Cexus, and T. Chonavel, "Some useful properties of cross--energy operator," AEU - International Journal of Electronics and Communications, vol. 63, pp. 728-735, 2009.

[39] Z. Saidi, A. O. Boudraa, J. C. Cexus, and S. Bourennane, "Time-Delay Estimation Using Cross Energy Operator," Internation Journal of Electrical, Robotics, Electronics and Communications Engineering, vol. 1, 2007.

[40] J. F. Kaiser, "Some useful properties of Teager's energy operators," in Acoustics, Speech, and Signal Processing, 1993. ICASSP-93., 1993 IEEE International Conference on, 1993, pp. 149-152 vol.3.

[41] J. F. Kaiser, "On a simple algorithm to calculate the `energy' of a signal," in Acoustics, Speech, and Signal Processing, 1990. ICASSP-90., 1990 International Conference on, 1990, pp. 381-384.

[42] F. Xiao, L. Dong, L. Li, and X. Liao, "A Novel Open-loop Frequency Estimation Method for Single-Phase Grid Synchronization under Distorted Conditions," IEEE Journal of Emerging and Selected Topics in Power Electronics, vol. PP, pp. 1-1, 2017.

[43] "IEEE Guide for Synchronization, Calibration, Testing, and Installation of Phasor Measurement Units (PMUs) for Power System Protection and Control," IEEE Std C37.242-2013, pp. 1-107, 2013.

[44] "IEEE Standard for Synchrophasor Measurements for Power Systems," IEEE Std C37.118.1-2011 (Revision of IEEE Std C37.118-2005), pp. 1-61, 2011.

[45] L. Jae-Duck, L. Seong-Joon, B. Jeong-Hyo, and K. Dae-Yun, "The PMU interface using IEC 61850," in ICT Convergence (ICTC), 2013 International Conference on, 2013, pp. 1125-1128.

[46] M. McGranaghan and G. Beaulieu, "Update on IEC 61000-3-6: Harmonic Emission Limits for Customers Connected to MV, HV, and EHV," in Transmission and Distribution Conference and Exhibition, 2005/2006 IEEE PES, 2006, pp. 1158-1161.

[47] "IEEE Draft Guide for Applying Harmonic Limits on Power Systems," IEEE P519.1/D12, July 2012, pp. 1-124, 2015.

[48] Y. Jiang and A. Ekstrom, "General analysis of harmonic transfer through converters," Power Electronics, IEEE Transactions on, vol. 12, pp. 287-293, 1997.

Chigozie J Nwobu (M'12) received the MEng/BEng degree in Electronic and Electrical Engineering from the University of Leeds in 2012 and a PhD in 2016 working with University of Leeds Control and Power Applications Group. His main research interests are power electronics, Grid Control, Static VAR compensators, MMC converter topologies, measurement techniques for power systems and Integration of energy storage.

Agnes M Nakiganda (M'15,) received her M.Sc. degree in Electrical Engineering and Renewable Energy Systems at the University of Leeds in 2015. Her Master's thesis was based some areas in this publication co-supervised by C.J. Nwobu and L. Zhang. Her research interests are in Active filtering, Grid synchronization Static VAR compensators. Currently, she is a lecturer Renewable Energy Systems at Busitema University in Uganda.

Li Zhang (M'93,) is a Senior Lecturer in Electrical Engineering and Renewable Energy Systems at the Electronics and Electrical Engineering department in the University of Leeds. Currently, she is the associate editor for the IEEE Transactions on Power Electronics and IET Proceedings on Power Electronics Journals. Her current research interests are in power converters for power system applications, FACTS devices (STATCOM, UPFC).